J. Fluid Mech. (2004), *vol.* 518, *pp.* 347–362.
DOI: 10.1017/S0022112004001235 Printed in the United Kingdom

The growth and structure of double-diffusive cells adjacent to a cooled sidewall in a salt-stratified environment

By LIORA MALKI-EPSHTEIN[1], OWEN M. PHILLIPS[2] AND HERBERT E. HUPPERT[1]

[1]Institute of Theoretical Geophysics, Department of Applied Mathematics and Theoretical Physics, Centre for Mathematical Sciences, University of Cambridge, Wilberforce Road, Cambridge, CB3 0WA, UK

[2]Department of Earth and Planetary Sciences, The Johns Hopkins University, Baltimore, MD, 21218, USA

(Received 21 January 2004 and in revised form 27 July 2004)

Observations and measurements are reported on the patterns and rates of growth in time of the double-diffusive cells that form adjacent to a cooled sidewall in a salt-stratified environment. Fluid near the wall is cooled and sinks a distance h where its density, increased by cooling, matches that of the salt-stratified ambient. The fluid separates from the wall, moving outwards as a cool, fresher layer beneath a warmer, more saline region. This leads to growing double-diffusive cells that advance outward at a rate, found by dimensional reasoning, to initially be proportional to N_0h, where N_0 is the initial buoyancy frequency in the ambient and h is the intrusion's vertical thickness. Near the wall at the top of each cell, the sinking colder fluid is continually replaced by selective withdrawal from the ambient 'far field'. The fluid being withdrawn from the ambient is always the least dense in the cell, and as the experiment proceeds, the straining of the fluid in the ambient region reduces the stratification. The vertical density gradient inside the cell relaxes by continuous hydrostatic adjustment (CHA) to match the ambient and the speed of advance reduces. Measurements of the rate of advance of the cell nose were made in tanks of different lengths L with a range of initial salinity gradients and temperature differences. A simple two-dimensional model is developed to describe the rate of extension of the cells and the internal density gradient as functions of time in which the tank length appears as an important variable. This effect does not seem to have been recognized previously. The rates of evolution in each run involve the time scale $\tau = L/(C_H h N_0)$, where $C_H \approx 10^{-2}$ is a heat transfer coefficient. The mean length of the cells $\bar{l}(t)$and the internal buoyancy frequency as functions of time are given by

$$\bar{l}(t)/L = t/\tau - (t/2\tau)^2, \quad N = N_0(1 - t/2\tau).$$

Inversion of the first of these expressions results in $t/\tau = 2 - 2\{1 - (\bar{l}(t)/L)\}^{1/2}$ from which a time scale τ^{-1} can be estimated. The measurements from individual runs when plotted in this way generally produce accurate straight lines as the model predicts, from which C_H is found. This should be approximately the same for each run; the mean over all runs was found to be 9.3×10^{-3} with standard deviation 2.4×10^{-3}. The velocity scale of the intrusions at the beginning of an experiment is of order $10^{-2}\,\mathrm{cm\,s^{-1}}$, for typical parameters of water at temperature 20 °C, cooled wall temperature of 0 °C and mean salinity of 5%.

1. Introduction

Double-diffusive convection arises when solutions with vertical gradients of two (or more) components having different molecular diffusivities (salt and heat, or sugar and salt for example) drive convective motions in a fluid that is overall gravitationally stable. The laboratory experiment of Ruddick & Turner (1979) on the growth and evolution of double-diffusive intrusions from an initially sharp vertical front between balanced gradients of salt and sugar provide a most beautiful example of complex, self-organizing fluid structures. The interplay between the double-diffusive transport inside each of a stack of cells and the internal circulation pattern, and the communication between cell pairs across diffusive interfaces is easy to admire but difficult to understand quantitatively. The self-organizing character of this flow impedes our efforts to derive a quantitative description of its overall dynamics–in seeking to understand how it works, how does one begin?

Some oceanic lateral intrusions found across thermohaline fronts in the vicinity of meso-scale eddies appear to be driven by density gradients maintained by double-diffusive processes of this kind (Ruddick 1992). From their laboratory measurements, Ruddick & Turner established the vertical scale of the cells as $g\beta(\Delta S)/N_0^2$, where $\beta(\Delta S)$ is the relative density contrast across the front due to salinity and N_0 the initial overall buoyancy frequency. Later, Ruddick, Phillips & Turner (1999) obtained some additional, but fragmentary, relations on the mean circulation velocity and finger flux ratio, but did not establish further quantitative relations.

Conceptually simpler experiments have been conducted by Thorpe, Hutt & Soulsby (1969), Chen, Briggs & Wirtz (1971), Huppert & Turner (1980), Chan, Chen & Chen (2002) and others. These involve a region of stably stratified salt solution at initially constant temperature, with heating or cooling then applied to one side, and this provides a clearly identifiable and controllable driving force for the motion. In each, a stack of cellular layers was found to develop adjacent to the heated or cooled wall, remaining generally constant in vertical thickness and extending outwards in time. In the case of a cooled wall, an element of fluid, initially at the ambient salinity and temperature, is cooled by the adjacent wall and its density increases by the amount $\Delta\rho_T \approx \rho_0\alpha\Delta T$, where α is the expansion coefficient and ΔT the temperature difference between the wall and the fluid. Since the diffusivity of heat is much greater than that of salt, a cooled fluid element can be considered to retain its salinity, and it is then denser than the ambient fluid at the same level. As it sinks down the wall, its (negative) buoyancy decreases relative to the stratified ambient at the same level until the two are matched at a distance h below, where

$$\Delta\rho_T \approx \left(-\frac{\partial\rho}{\partial z}\right)_0 h = \frac{\rho_0 N_0^2 h}{g}.$$

At this level, the colder, fresher fluid near the cooled wall is neutrally buoyant relative to the ambient at the same level, so that it moves out, approximately horizontally, and the balance above leads to the vertical height scale for the cells

$$h \approx \frac{\Delta\rho_T}{(-\partial\rho/\partial z)_0} = \frac{g'}{N_0^2} \tag{1.1}$$

where $g' = g\Delta\rho/\rho_0 \approx g\alpha\Delta T$. This vertical scale was confirmed experimentally by Chen *et al.* (1971) and by Huppert & Turner (1980) for Rayleigh numbers up to 10^9.

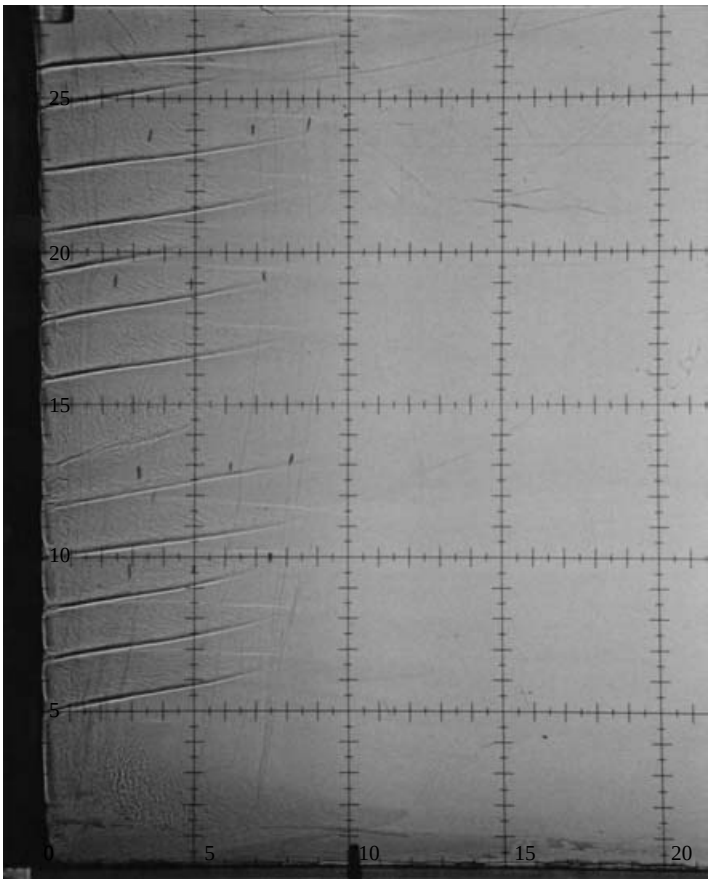

FIGURE 1. A shadowgraph image of the developing cells after 7 min. The larger grid squares are 5 cm on a side. Variations in refractive index resulting from salinity variations, which diffuse only slowly, produce stronger images than do more diffuse temperature variations. The inclined lines indicate salinity boundaries, with cooler, fresher water above more saline ambient water.

The original position of the fluid near the wall must be re-occupied by uncooled fluid drawn from the stably stratified environment at the same general level, as in the 'selective withdrawal' from a stratified reservoir, described by Imberger, Thompson & Fandry (1976). The subsiding, chilled fluid near the wall reaches its new equilibrium level and moves outwards, essentially horizontally but rising a little as it begins to warm by thermal diffusion from the fluid below. When the wall is heated, rather than cooled, the sense of the circulation in each cell is reversed. This much is clear from the Huppert–Turner experiment – the heat transfer from the sidewall is the engine that drives the circulation. Figure 1 is a shadowgraph image of the layers in a typical experiment at the stage where the double-diffusive cells have formed and are beginning to extend outward.

The fact that there is a clear, controllable energy source in these experiments provides a starting point for a simple but quantitative description of the physical balances involved and the flow that appears. In this paper, we describe more extensive and detailed observations of the flow pattern, with measurements of the growth of

the cells in terms of the ambient initial stratification and the wall cooling. During the course of these measurements, we discovered that the rate of growth of the cells was not constant but decreased monotonically during the experiment. This is illustrated in figure 2(*a*), which shows experimental data for the average length of the intrusions as a function of time, for a single experiment partitioned into two parts by positioning the cooling plate within the tank. This resulted in two identical experimental runs in the parameters of temperature difference and stratification, but with different tank lengths, one 48 and the other 147 cm long. After about an hour, the intrusions in the short part have begun to slow noticeably, compared with those on the long side. Therefore, the growth of the intrusions is found to depend on the length of the tank.

We further realized that as each experiment proceeded in a tank of necessarily finite length, the entrainment of fluid from the ambient 'far field' into each cell produced, in the ambient region, an increasingly stepped density profile from the initially uniform 'far field' stratification. Thinner layers of larger density gradient at the heights of selective withdrawal separated deeper layers of reduced gradient over levels corresponding to the double-diffusive cells. As the experiment proceeded, these reduced gradients (and consequently the buoyancy frequency N) continued to reduce further, as did the rate of growth of the cells themselves, as shown in figure 2(*a–c*). The modification of 'far field' conditions was observed by particle tracking to commence at the beginning of the experiment and continue throughout as the cell noses approach the far end of the tank. The size of the reservoir, the experimental tank, dictates how quickly this density structure changes and, consequently, how fast the intrusions propagate. This effect of finite tank length in experiments on spreading double-diffusive cells does not seem to have been recognized explicitly before.

The relation between the initial growth rate of the cells and the two external quantities: the temperature difference between the fluid and the wall, and the internal density gradient, is evident from dimensional reasoning. Let us assume that the cell growth is governed by the local heat transfer and cell dynamics, in which the cell height h (which is a function of the temperature difference) and internal stratification parameter N_0 are the only relevant length and (inverse) time scales. Dimensional reasoning then indicates that the only velocity scale is hN_0, alternatively expressed as $\alpha\Delta T(g\rho_0)^{1/2}(\mathrm{d}\rho/\mathrm{d}z)^{-1/2}$. The nose velocity of the cells is found experimentally to be consistent with this scale, with a constant of proportionality of order 10^{-2}, but it is also found to decrease with time.

A more detailed but still simple model developed below contains only one experimentally determined parameter, in essence a heat transfer coefficient, and this will be found to provide the factor of proportionality 10^{-2}. The predictions of the model are found to compare well not only with the measurements of cell length, but also with our observations of the evolution of the density field from its initially smooth gradient towards a series of steps with thin regions of high gradient separating the cells. In the cells themselves, and in the ambient regions at the same level, the density gradient decreases continuously as the cells extend across the tank. These observations will be discussed in a subsequent publication, and are also described in detail in Malki-Epshtein (2005).

2. Experimental methods

Three different tanks were used in the experiments, all 7.5 cm wide and made of Perspex, 1.1 cm thick, with internal lengths and depths of 50 cm × 30 cm, 200 cm × 22.3 cm and 232.5 cm × 40 cm. Most experiments were insulated using polystyrene

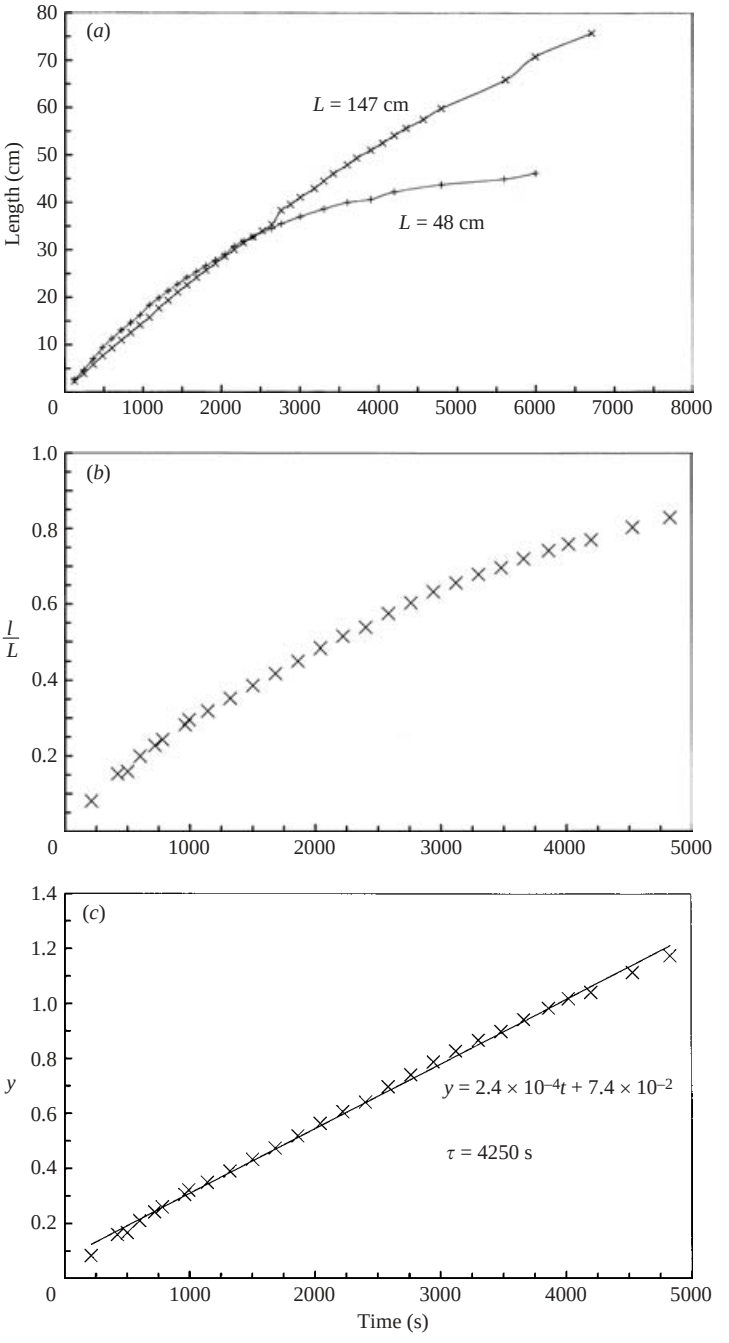

FIGURE 2. (*a*) Length as a function of time for run 19 (see table 1), which was partitioned by the double-sided cooling plate into two tanks of length 48 and 147 cm. Both tanks have exactly the same initial stratification and temperature difference, yet the growth in time of the average length of the layers is clearly different. Initially both sides developed alike, having a comparable number of layers, positioned at comparable heights, and advancing with comparable initial velocities. As time progressed, the intrusions diverged and propagated at different speeds. (*b*) The dimensionless mean length of the cells, $l(t)/L$, as a function of time in run 1, showing the decrease in time of the growth rate. (*c*) The same data from run 1 are plotted as in equation (4.11) with $y = 2 - 2(1 - \bar{l}(t)/L)^{1/2}$ plotted against time. The time scale of the cell growth is the inverse slope of the best-fit line, in this instance 4250 s.

Expt.	L (cm)	T_0 (°C)	ΔT (°C)	Ra ($\times 10^5$)	N_0 (s^{-1})	$\bar{h}$ (cm)	τ (s)	v_0 ($\times 10^{-2}$ cm s^{-1})	C_H ($\times 10^{-3}$)
1	48.2	20.3	20.3	7	1.47	1.1	4250	1.1	0.7
3	48.2	20	20.3	40	0.85	2.6	1810	2.7	1.2
4	48.2	20.9	26	120	0.83	2.6	1760	2.7	1.3
8	48.2	20.5	20.3	20	1.18	1.5	2250	2.1	1.2
15	48.2	22	15	40	0.75	2.8	1980	2.4	1.2
18	48.2	21.7	21.7	50	0.89	2	2660	1.8	1.0
19L	48.2	20.1	20.1	7	1.12	1.4	3130	1.5	1.0
19R	147	20.1	20.1	7	1.12	1.6	10790	1.4	0.8
21	232.5	17.5	26	10	1.21	1.4	23140	1.0	0.6
22	232.5	18	18	9	0.91	1.7	23360	1.0	0.6
23R	116.5	19.3	18	20	0.89	1.6	8800	1.3	0.9
23L	116.5	19.3	18	20	0.89	1.6	8980	1.3	0.9

TABLE 1. Summary of data on cell growth. The columns are, respectively: experiment number; tank length; initial water temperature; temperature difference between water and cooling plate; Rayleigh number; initial buoyancy frequency; mean vertical thickness of the cells; time scale τ of the experiment found from the data plotted as in (4.11); initial velocity scale inferred from τ; and heat transfer coefficient inferred from τ.

blocks, but no qualitative differences in the results were found in those that were not insulated, possibly because of the already thick Perspex walls and the generally modest temperature differences used. For each run, an initially uniform salt stratification was produced with a conventional double-bucket system and the gradient was measured before the start of each experiment using a refractometer with samples extracted at 2 cm vertical intervals by a fine syringe. A 1.8 cm wide copper plate cooled by chilled water circulating through it was installed in the tank, usually at one end. A few experiments were conducted with the (double sided) cooling plate at an interior cross-section. Shadowgraph imagery was used routinely.

Most experiments were carried out in the smaller 50 cm × 30 cm tank. In a normal run, within one or two minutes of the initiation of cold-water flow into the cooling plate, the adjacent downwards flow could be seen to separate and move away from the wall, forming the bottom of the outwardly growing cell. The nose of each cell and the salinity contrast at the bottom of the developing doubly-diffusive region were usually very clear after the first five minutes or so, and the progression of the cell nose as it advanced was measured at frequent intervals. In the smaller tank, the nose would reach the endwall after a time of order one hour, but in the longer tanks, measurements were continued for a couple of hours, by which time the cell noses had crossed about one-third of the tank. The vertical thickness h of the individual layers was measured several times during each run; it frequently varied among the layers by up to 15%, but the means remained more stable. In some runs, injected particles were tracked or potassium permanganate crystals were dropped through the cells to delineate qualitatively the nature of the internal circulation. In all, 12 satisfactory experimental runs were made with the parameters specified in table 1. The duration over which the cell evolution was measured ranged from 45 to 120 min, the initial density gradients $\rho_0^{-1}(\partial\rho/\partial z)$ ranged between (0.58 and 2.34) $\times 10^{-3}$ cm^{-1} ($N_0 \approx 0.75$ and 1.52 s^{-1}), ambient-to-cooling plate temperature differences from 10 to 26 °C and tank lengths as given above.

3. General flow characteristics

From the flow visualizations mentioned above, we confirm that the general structure of the flow involves a stack of largely uncoupled cells, separated vertically by the selective withdrawal layers mentioned earlier, each driven by the sinking of cooled, denser water in an unsteady but low-Reynolds-number layer adjacent to the cold plate. Eddies with scales of order 0.5–1.0 cm but containing little fine structure, roll randomly down the plate to the base of each cell, then separate from the wall and move generally outwards. Particularly in the first few minutes of the experiment, some cooled fluid could be seen to rebound somewhat before settling. The downward volume flux is supplied by 'selective withdrawal' inflow from the ambient region towards the plate in a relatively thin layer at the top of each cell, which appears very clearly in figure 3(*a*, *b*). Both are photographs taken at advanced stages of an experiment run in the 232 cm tank, where the cooled wall is on the left and the intrusions are advancing towards the right. Earlier in this experimental run potassium permanganate crystals had been dropped both through the developing intrusions and at the far end of the tank. In figure 3(*a*) the potassium permanganate has dispersed through the entire mixing region of each cell. A second dye streak was injected a few minutes before this photograph was taken. Between each pair of cells is the clear selective withdrawal layer in which unstained fluid moves inwards from the far field, its boundaries remaining sharp because of the smallness of the salt diffusivity (ca. 1.3×10^{-5} cm^2 s^{-1} at 20 °C, about 80 times smaller than that of heat, 1.47×10^{-3} cm^2 s^{-1}, and 600 times smaller than the diffusivity of vorticity, i.e. the kinematic viscosity, ca. 10^{-2} cm^2 s^{-1}). The level of the withdrawal layer can be seen in figure 3(*a*) to drop slightly as the fluid being withdrawn cools by thermal diffusion from the cells above and below. In figure 3(*b*) the intrusions can be seen advancing from the left. The initially straight vertical dye streak at the far end of the tank remains sharp due to virtually no diffusion or mixing in this region. The dye streak has been altered by the horizontal flow, which had transported the dye along with the fluid towards the intrusions in the withdrawal layer and away from them ahead of the cells. The resulting periodic structure can be seen, at the bottom of the photograph, to be consistent with the positions of the intrusions (being just out of phase). Some intrusions in the middle region were less developed and had advanced much less than the others, and correspondingly the ambient flow in that region was weaker and resulted in less deformation of the dye streak.

In the boundary layer along the cooling plate, the volume flux in each cell is downward between what are essentially stagnation points at the levels of selective withdrawal. As the cell volume increases and displaces ambient fluid, since the tank length is finite continuity requires a general upward drift at the far end of the tank to compensate. The internal Froude number in these experiments $U/Nh \approx 10^{-2}$ is very small, so that the ambient density distribution, though changing slowly as a result of the withdrawal, remains close to hydrostatic equilibrium, with less-saline fluid at the top level of each cell. It is important to remember that the fluid being selectively withdrawn in each cell from the ambient is always the least-saline water in that cell; it sinks down the wall because here it is also the coldest. In a typical experiment, the observed withdrawal layer thickness was about one third the vertical height of an individual cell. Imberger *et al.* (1976) show in a similar low-Froude-number flow, that the withdrawal layer is steady with thickness of order $LG_r^{-1/6}$, where $G_r = N^2L^4/\nu^2$, is the Grashof number. Applying these results to our study, with tank lengths between 0.5 and 2 m and a Grashof number of about 4×10^{12}, suggests a vertical thickness of the withdrawal layer at the far end of about 0.8 cm, which is in accordance with our observations.

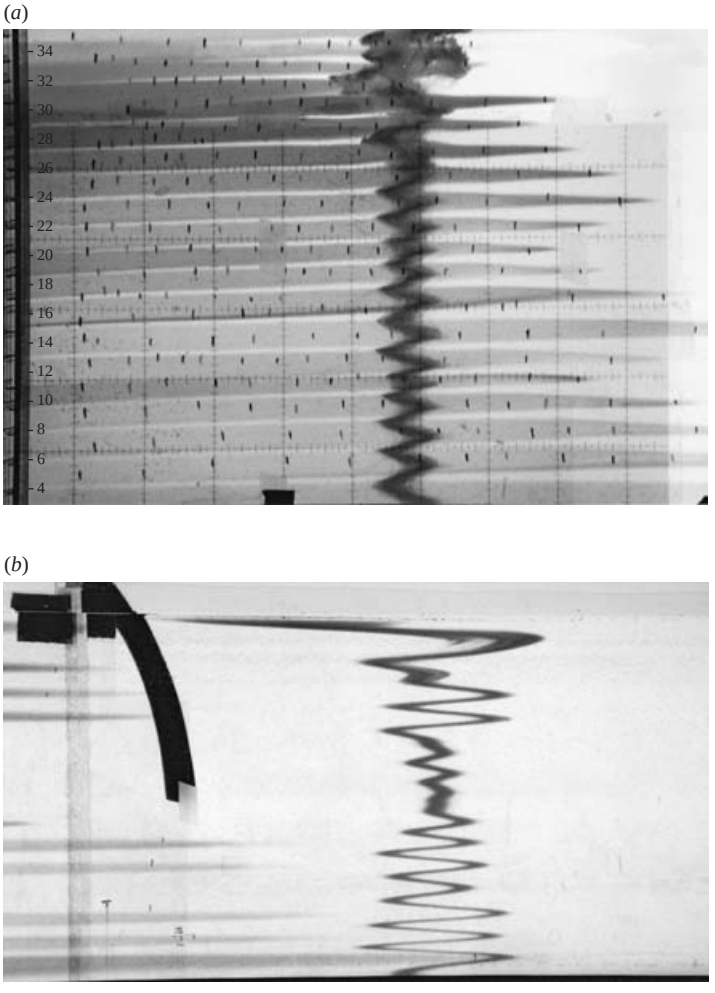

FIGURE 3. The cell pattern and ambient region flow in the 232 cm tank at an advanced stage of growth, where the cooled wall is on the left and the intrusions are advancing to the right. Earlier in the run, potassium permanganate crystals were dropped at the far end of the tank, and through the stack of cells where the dye has diffused throughout the double-diffusive regions. (*a*) The region of the intrusions. A second dye streak was injected a few minutes before this photograph was taken and has become zig-zagged in the flow. Between each pair of cells, clear water is being selectively withdrawn from the ambient, and is moving to the left towards the cooling plate. Note the absence of mixing in this part of the flow, and the gradually decreasing level of fluid being withdrawn as it becomes cooler (by molecular conduction from above and below) and denser. The ticks identify the locations of the cell noses at various earlier times in the experiment. (*b*) The flow pattern at the far end of the tank, and the intrusions can be seen advancing from the left. The initially straight vertical dye streak at the far end of the tank remains sharp due to virtually no diffusion or mixing in this region. The dye streak has been altered by the horizontal flow, which had transported the dye along with the fluid towards the intrusions in the withdrawal layer and away from them ahead of the cells. The resulting periodic structure can be seen, at the bottom of the photograph, to be consistent with the positions of the intrusions (being just out of phase).

When the boundary layer fluid separates and moves away from the wall, it is colder but fresher than its surroundings above and below. Its salinity contrast with the fluid just below produces the dark lines in figure 1, sloping upwards as the fluid warms by thermal diffusion while remaining relatively fresh, since the salt diffusivity is relatively so small. The lower side of this flow, with cool fresher water above warm more-saline water is locally stable; the salinity contrast remains sharp and is visible clearly in the shadowgraph imagery. The upper side, with warm saline water above cool fresher water is unstable, producing double-diffusive fingers. In the experiment, it was difficult to discern any long steady fresher-water fingers that might have been present, but observations with small injected particles showed that there was a general upwards drift from the discharge layer with rather irregular small-scale structures superimposed. A structure of steady double-diffusive fresher sheets or fingers rising through a stable temperature gradient has been shown by Howard & Veronis (1992) to be dynamically unstable, and by Knoblock, Proctor & Weiss (1992) to degenerate into chaos. On the other hand, in a flow like ours but with a heated (rather than cooled) sidewall, Chan *et al.* (2002) have used particle imaging velocimetry to identify secondary counter-rotating mean vortices in the layers, with velocities of order half that of the overall circulation. These prior results are consistent with our inability to discern the more regular finger structure usually observed in convecting interfaces (see e.g. Shirtcliffe & Turner 1970).

The circulation inside each cell is fed by the 'processing' of an ever-increasing volume of fluid drawn into the boundary layer and cooled, so that the cell volume and length continually increase with time, albeit at a decreasing rate as the experiment proceeds. In kinematical terms, when fresh-water fingers infiltrate up into a stratified region that is at rest and connected with a large stratified ambient, the water being displaced tends to move away horizontally. Fluid in the fingers moves vertically upward, but the cold, fresher layer supplying them from below is a barrier to any net vertical volume flux of the interstitial fluid among the fingers. In laboratory coordinates, then, the macroscopic Eulerian mean velocity, averaged over a domain large compared to the finger scale yet small compared to the cell scale, is upward from the fresher layer and outward, away from the cooled wall. In terms of the overall circulation, the outward flow compensates for the fluid being extracted from the 'far field' near the top of the cell in the selective withdrawal.

It has already been pointed out that the internal Froude number is very small, and the mean overall density distribution is very close to hydrostatic equilibrium, or 'horizontally compensated' in oceanographic terms (Rudnick & Mattin 2002). This constraint provides an important tool for the interpretation of these observations. In general, a sudden perturbation from equilibrium produces restoring forces that move the system back towards equilibrium in a time scale N^{-1}. But in a double-diffusive situation, the temperature and salinity of a macroscopic fluid element (and consequently its density) may vary over time scales large compared than N^{-1} as a result of the differential fluxes of heat and salt, whether or not macroscopic thermal conduction is neglected. As the density of fluid elements change, their vertical location adjusts as they drift to maintain overall hydrostatic equilibrium. This produces a gradual and continuing evolution of the density field, a process Ruddick *et al.* (1999) call 'continuous hydrostatic adjustment' (CHA).

Although the field as a whole is very close to hydrostatic adjustment, local departures from hydrostatic equilibrium accompany the sloping isohalines that produce the dark lines in figure 1 and the downwards sloping withdrawal layers in figure 3(*a*). These are sites of vorticity generation. The balance of mean vorticity in a

two-dimensional flow is governed by (Phillips 1977)

$$\frac{\mathrm{d}\omega}{\mathrm{d}t} = -\rho^{-2}\,\nabla p \times \nabla\rho + \nu\nabla^2\omega \tag{3.1a}$$

$$= \rho^{-1} g(\partial\rho/\partial x) + \nu\nabla^2\omega, \tag{3.1b}$$

where the rate of generation of vorticity is represented by the term involving the horizontal density gradient (the 'baroclinic effect' in meteorology) where isopycnals slope relative to the horizontal. In the experiments, the salinity jump sloping upward to the right in figure 1 must be a local source of clockwise vorticity, while in the selective withdrawal layer the nearly horizontal isopycnals must converge towards the cooling plate as the flow accelerates. Outside these structures, the smallness of the internal Froude number implies that macroscopic motions produced by double-diffusive fluxes are the result of CHA. This ensures that the isopycnals are essentially horizontal and that, except for the molecular diffusion of vorticity (mainly horizontal shear), the mean drift flow field is irrotational, or pure strain. The qualification is important in these experiments with cell thickness h of order 3 cm and viscosity ν of $10^{-2}\,\mathrm{cm^2\,s^{-1}}$, since the vorticity diffusion time $h^2/2\nu$ is less than 10 min, short compared with the duration of the experiment. The distribution of mean vorticity in the experiment (cf. the dye traces in figure 3) is then largely a consequence of local generation and cancellation of vorticity of opposite signs at different levels, with vertical diffusion between them. In the ambient or outside region, flow is induced by the extension of the cooled convecting finger region but there is no mixing, so that the isopycnals move with the fluid. As the 'finger region' extends towards the far tank wall (not necessarily uniformly over the height of the cell), the horizontal convergence in the outside region is balanced by vertical divergence between the bottom of the cell and the selective withdrawal region at the top.

4. The elongation of the cells and evolution of the density field

The qualitative observations above provide the bases for a simple but quantitative two-dimensional model whose results concerning the rates of cell growth and the evolution of the density and temperature fields can be compared with those from the experiment. It has three primary ingredients.

The first is the cooling-layer heat balance. Let q represent the volume flux withdrawn from the ambient region and circulated through the cooled layer along the boundary and let δT be its temperature decrease. The rate of heat loss per unit width of a cell, that is advected away by the volume flux q, i.e. $\rho c_P q\delta T$, is usually parameterized by the heat transfer formula $C'_H \rho c_P w \Delta T h$, where w is the mean velocity down the surface in the cooling layer, ΔT the maintained temperature difference between the ambient fluid and the cold wall, and c_p the specific heat. The heat transfer coefficient C'_H in turbulent free convection at relatively low Reynolds numbers is generally of order 10^{-2} (Goldstein 1938, Ch. 15). With a smooth surface, the temperature profile in the thermal conduction layer adjacent to the wall is very steep, so that the average temperature decrease δT of the circulating, more turbulent fluid, though proportional to the total difference across the layer, is in magnitude only about half of it. Accordingly,

$$q\delta T = C'_H w \Delta T h \propto C'_H w \delta T h,$$

and the volume flux in the selective withdrawal layer and down the wall boundary layer

$$q \propto C'_H w h. \tag{4.1}$$

Note that the smallness of C'_H implies that the mean velocity w down the cooled wall and the cell height h are large compared respectively with the fluid velocity in selective withdrawal and the thickness of the withdrawal layer. Our visual observations were consistent with this.

Secondly, consider the balance of vertical momentum down the cooled layer. This contains a driving buoyancy term $g\alpha\delta T \sim N^2 h$, an inertial/Reynolds stress term of order w^2/h and a viscous term of order $\nu w/\delta_x^2$, where δ_x is the cooled layer thickness. In the experiments, N, h and w in c.g.s. units are all of order unity, so that the viscous term would be significant in the balance only if the layer thickness were of order 1mm or less, much smaller than observed. Consequently we must have $N^2 h \propto w^2/h$, and

$$w \propto Nh. \tag{4.2}$$

A simple physical interpretation of this expression can be given in terms of the recovery rate of a disturbance back to hydrostatic equilibrium. Fluid elements in the selective withdrawal layer have a density that is in equilibrium at the top of the cell. On approaching the wall, they are chilled and their density decreases so that their new equilibrium level is a distance h below, as Huppert & Turner (1980) showed. The time scale for recovery of their hydrostatic equilibrium is N^{-1} (the effect of laminar or turbulent viscosity being to damp any oscillation) so that the vertical velocity w down the cooled wall is the distance h divided by this time scale, which again gives (4.2).

The proportionality statements (4.1) and (4.2) can now be combined, and at the same time, we incorporate the $O(1)$ constants of proportionality into C'_H; writing the resulting modified heat transfer coefficient as C_H, whose magnitude is to be determined experimentally (though we still expect it to be $O(10^{-2})$), we obtain

$$q = C_H N h^2. \tag{4.3}$$

Finally, we consider the kinematics of deformation of the outer ambient fluid by the extending finger region. It was pointed out earlier that the horizontal convergence of the linearly stratified ambient region is balanced by vertical divergence between the bottom of the cell and the selective withdrawal layer at the top. Although the horizontal convergence in the ambient may not be uniform across the depth of the cell as the active double-diffusive region deforms, the fluid being selectively withdrawn at the top is always from the least-dense layer in the ambient region of that cell.

Suppose that, at some height z above the base of the cell, the double-diffusive region extends a distance $l(z, t)$ from the cooling wall, beyond which the ambient fluid is salt-stratified and essentially non-diffusive. In this latter region, consider the deformation following the motion of the horizontal incremental layer of length $L - l(z, t)$ and volume $\mathrm{d}V = \{L - l(z, t)\}\,\mathrm{d}z$. The difference in fluid salinity between the bottom and the top of this non-diffusive layer is conserved, so that

$$\mathrm{d}S = \frac{\partial S}{\partial z}\,\mathrm{d}z = \frac{\partial S}{\partial z}\frac{\mathrm{d}V}{\{L - l(z,t)\}} = \left.\frac{\partial S}{\partial z}\right|_0 \frac{\mathrm{d}V}{L},$$

since at time $t = 0$, $l(z, 0) = 0$ and $\mathrm{d}V/L = \mathrm{d}z$. Thus

$$\frac{\partial S}{\partial z} = \left.\frac{\partial S}{\partial z}\right|_0 \frac{L - l(z,t)}{L}. \tag{4.4}$$

As the double-diffusive region grows and $l(z, t)$ increases, the ambient vertical salinity gradient decreases, though not uniformly, since we observe that l varies with z. A vertical integration of equation (4.4) yields $S_1(t)$, the salinity of the withdrawal layer

relative to that at the base of the cell S_0,

$$S_1(t) - S_0 = \left.\frac{\partial S}{\partial z}\right|_0 \int_0^{\Delta z} \{1 - l(z,t)/L\}\,\mathrm{d}z.$$
$$= h \left.\frac{\partial S}{\partial z}\right|_0 \left(1 - \frac{\bar{l}(t)}{L}\right)$$
$$= h \left.\frac{\partial S}{\partial z}\right|_0 \left(1 - \frac{V_{DD}(t)}{V_T}\right), \tag{4.5}$$

where $\bar{l}(t)$ is the mean length of the doubly diffusive region at time t and $V_{DD}(t)/V_T$ is the fraction of the total tank volume that it occupies. Since $S_1 < S_0$ and the vertical salinity gradient is negative, the form of (4.5) shows that S_1 increases towards S_0 in direct proportion to the fraction of fluid 'processed', regardless of the shape that the double-diffusion region assumes. According to CHA, the mean density gradient throughout the cell is the same as it is in the ambient region, i.e. $\rho_0\beta[S_1(t) - S_0]/h$, even though in the cells it is supported by both temperature and salinity gradients in the double-diffusion region. Consequently, in each cell, the density gradients decrease equally from the initial value in both the ambient and the double-diffusive region. We can therefore write

$$N^2/N_0^2 = 1 - \bar{l}(t)/L, \tag{4.6}$$

throughout. Note that since $q = h(\mathrm{d}\bar{l}/\mathrm{d}t)$, we have, from (4.3),

$$\frac{\mathrm{d}\bar{l}}{\mathrm{d}t} = C_H N h, \tag{4.7}$$

which is in accordance with the similarity reasoning in the introduction. Differentiation of equation (4.6) and incorporation of (4.7) gives

$$\frac{\mathrm{d}\bar{l}}{\mathrm{d}t} = -\frac{2LN}{N_0^2}\frac{\mathrm{d}N}{\mathrm{d}t} = C_H N h,$$

whence

$$\frac{\mathrm{d}N}{\mathrm{d}t} = -\frac{C_H h N_0^2}{2L} = -\frac{N_0}{2\tau}, \tag{4.8}$$

say, where the cell evolution time scale τ, which is found to be an important parameter in the data analyses, is given by $\tau = L/(C_H h N_0)$. Since $\bar{l} = 0$ and $N = N_0$ at time $t = 0$, we have from (4.8) and (4.6) that

$$N = N_0\{1 - (t/2\tau)\}, \tag{4.9}$$

so that the mean buoyancy frequency in the cell interior (and consequently, by CHA, at the same levels throughout the tank) decreases linearly in time. Also, for the mean length of the cells

$$\bar{l}(t)/L = t/\tau - (t/2\tau)^2, \tag{4.10}$$

where $\bar{l}/L = 1$ when $t = 2\tau$, at which time also, from (4.9), the internal density gradient in the layers vanishes (producing the stepped density gradients that are familiar in the context of double-diffusive layers). Equation (4.10) can be inverted to give

$$\frac{t}{\tau} = 2 - 2\left(1 - \frac{\bar{l}(t)}{L}\right)^{1/2}, \tag{4.11}$$

a form that we find useful in analysis of the experimental data.

These model results are couched in terms of the mean length of the double-diffusive cells, the volume divided by the respective height. By far the most convenient observable is the distance of the nose from the cold plate, and it is the growth of this quantity that was measured in the experiments. Because of the approximate geometrical similarity observed in the shape of the double-diffusive region as it develops, the growth of the overall length should be proportional to the growth of the mean length, but not precisely equal to it for several reasons. One is that the region of double-diffusion is approximately triangular for reasons discussed earlier, so that the distance to the nose is greater than the mean. Also, as fresher colder fluid moves away from the boundary region and enters the double-diffusion region from below as rising cold fresh fingers or drops, some fraction of ambient fluid will be retained among them. This tends to make the volumetric rate of increase of the double-diffusive region greater than the rate of entry of the fresher processed fluid. On the other hand, at the top, fluid previously chilled but which by then has become warmer, may possibly be swept from the double-diffusive region into the withdrawal layer and recycled. This reduces the net rate of increase of double-diffusive cell volume. It is difficult to anticipate the net effect of these processes which work in opposite directions, but we do notice from the experimental results that the growth rate of the cells has decreased markedly by the time the nose length is approaching the far end of the tank, as seen in figure 2. This suggests that these various effects approximately balance. Consequently, and because the cooling layer thickness is small, we will interpret $\bar{l}$ in the expressions above as the distance of the cell nose from the cooling plate. On the other hand, at the beginning of each experimental run, it did take a few minutes for the flow to gather itself into the distinct cells that the model considers, so that a virtual time origin is allowed for the data analyses.

A similar experimental and theoretical study was conducted by Jeevaraj & Imberger (1991), who present an accompanying theory which takes into account the shape of the intrusions, which they infer from velocity and temperature profiles. Their results were interpreted as supporting the theory that the intrusion length varies as $t^{1/4}$ and is independent of the length of the tank. Our experimental results are not consistent with their suggestions.

5. Measurements of the rates of cell growth

The most revealing way to compare the experimental results to our simple model is by means of equation (4.11). According to this, a plot of $y = 2 - 2\{1 - \bar{l}(t)/L\}^{1/2}$ *vs.* t should produce a straight line with slope τ^{-1} and an intercept at $y = \bar{l} = 0$ that defines the virtual time origin t_0 for each run. An estimate of $\bar{l}(t)$ for any given experiment was obtained by averaging measurements of several intrusions at each time. Most of the experiments produced very good straight lines, as illustrated in figure 2(*c*) and in figure 4 for several other runs, which is satisfying in view of the simplicity of the model. In four of the 12 runs the experimental points wandered below the initial straight line after 30–50 min, possibly because of unwanted heat transfer through the sides of the tank. In such cases, the errant points from the later times in the experiments were discarded and a least-squares fit found over the previous nearly linear set. From the slopes of these lines, the time scale τ was found for each run, and the results are shown in table 1. The scale of the initial nose velocity v_0 for each run, estimated directly from $\bar{l}(t)$, is also listed in table 1. Values of v_0 were of order $10^{-2}\,\mathrm{cm\,s^{-1}}$.

With use of the measured parameters L, h and N_0, we calculated the 'heat transfer coefficient' $C_H = L/(\tau h N_0)$ (which includes the various $O(1)$ proportionality factors),

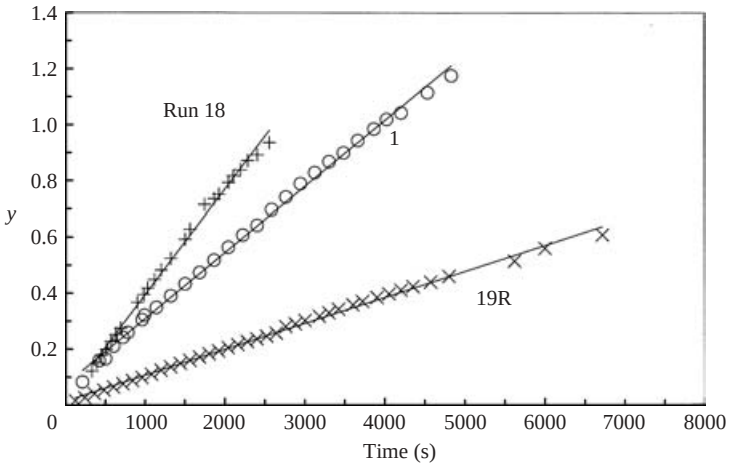

FIGURE 4. Least-squares fits for the 'inverse plots', with $y = 2 - 2(1 - \bar{l}(t)/L)^{1/2}$ plotted against time (cf. equation (4.11)), for some representative experiment runs.

shown in the last column of table 1. Although the precise magnitude of this coefficient is of limited interest per se, we would expect it to be essentially the same for all the experimental runs, except for experimental errors and possibly Reynolds and Nusselt number effects. The degree to which it agrees among the individual experimental runs is then a useful consistency check of the whole set. The values given in the table have a mean of 9.3×10^{-3} and standard deviation of 2.4×10^{-3}. The two runs in the long 232.5 cm tank both produced low coefficients, possibly because of lateral heat transfer or possibly from viscous thickening of the long selective withdrawal layer. Without them, the mean is 10^{-2} and standard deviation 2×10^{-3}, which is not very different. Some amount of scatter in the heat transfer coefficient is to be expected since the experiments covered a large salinity range, and many parameters such as viscosity, thermal expansion and heat diffusivity are strongly dependent on salinity.

Figure 5 presents a summary plot of $l(t)/L$ against t/τ, using the respective time scales and virtual origins as determined above. Results from experiments with different tank lengths are distinguished by different symbols; those from the longest tanks are concentrated towards the origin. The grouping of these results and the approximate consistency among the runs of the numerical values of C_H for quite different tank lengths and moderate ranges of N_0 and h (determined by the temperature differences) gives confidence both in the experiments themselves and also that the simple model is robust.

Finally, the cell growth is accompanied by the reduction in the internal density gradient and buoyancy frequency specified in the model by (4.6) and (4.9). Preliminary measurements have confirmed the emergence of increasingly 'steppy' salinity and density profiles in the far field, and, by inference, throughout the tank. These will be the subject of more detailed investigation in a subsequent paper.

6. Some concluding remarks

It is perhaps a little surprising that such a simple model can account accurately for the rate of cell growth and the evolution of the internal temperature and density fields. Several factors have made this possible. The most important is that we have restricted ourselves to those characteristics of the cells that are governed by the

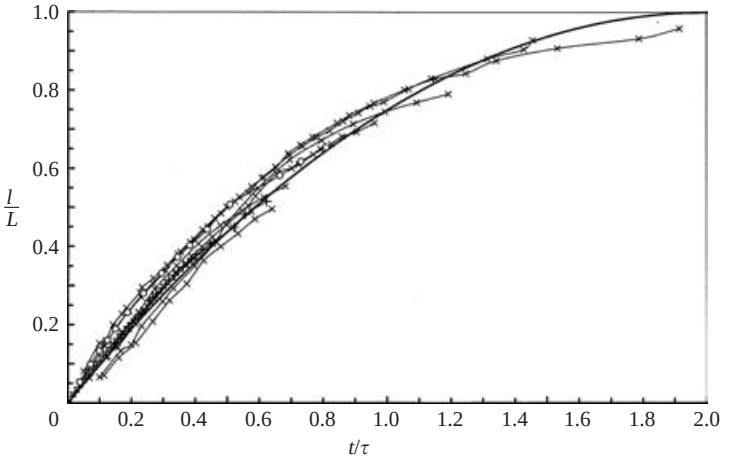

FIGURE 5. $l(t)/L$ as a function of t/τ, incorporating results from several experiments in tanks of three different lengths, marked according to the length of the tank as: $\times$, $L = 48.2$ cm; $\circ$, $L = 116.5$ cm, and $+$, $L = 147$ cm. The last set of points, difficult to see, is clustered close to the origin.

powerful constraint that the pressure field remains very close to hydrostatic in this very low-Froude-number flow, except possibly in the cooling layer at the plate. The vertical density profile has to be very nearly the same along the tank at all times, no matter what combination of temperature and salinity produces it. The overall straining of the 'far-field' stratified fluid tends to modify its density distribution, but continuous hydrostatic adjustment to the shape of the internal double-diffusive region keeps the density field close to hydrostatic equilibrium with the straining external field. The cell shape continually adjusts. However, the result (4.5) is independent of the shape of the double-diffusive region. It asserts that the salinity of the fluid being extracted from the 'far field' and processed in the cooling layer increases in direct proportion to the volume of fluid already processed. Its immediate corollary, (4.6), is the crucial link in the logic that binds together the evolution of overall state to the heat and momentum balances in the cooling layer driving the flow.

Secondly, the heat balance in the cooling layer involves two temperature differences– that between the cooling plate and the ambient fluid outside it and that between the fluid entering and leaving the cooling region. These temperature differences both vary throughout each experiment, but fortunately it can be argued reasonably that they remain proportional. As a result, they drop out of the cooling layer heat balance and do not appear explicitly in (4.1), although they do, implicitly, through h. However, an alternative and simpler approach makes these considerations irrelevant. If one is prepared to accept the similarity argument in the Introduction that the cell growth is governed by local dynamics, then we have immediately that $\bar{l}(t) \propto N(t)h$ (though we do not have the association of the proportionality constant with the heat transfer coefficient). With the kinematical expression (4.6), the principal results follow.

One minor problem with the experiment was that occasionally two adjacent cells would coalesce during a run to produce a thicker cell that would continue to evolve. The initial thickness of the cells was governed in (1.1) by the ratio of the density increase due to cooling by ΔT, and the ambient density gradient. As we have seen, both of these quantities decrease in time; the density gradient decreases as $(1 - t/\tau)^2$ and the density increase from cooling does so apparently less rapidly, possibly resulting

in a gradual increase in the thickness scale, and, apparently, the observed occasional readjustment.

The Huppert & Turner (1980) experiment was designed to elucidate the flow produced by a melting iceberg in an otherwise uncontained stratified environment. As $L \to \infty$ in (4.10), the speed of advance of the cells becomes constant and $\bar{l}(t) \to C_H h N_0 t$. The heat flux per unit area across the cooled wall remains $C'_H \rho c_p N_0 h \Delta T$, though in the oceanographic context additional effects of differential current velocities and windage may also play a role in the double-diffusive cell patterns. On the other hand, for appropriate parameters, the experimental results may be applicable directly to a compositionally stratified magma chamber with cooler walls, in which the time scale for layering to develop is simply τ, as given in § 4.

The authors are grateful to Professor J. S. Turner for helpful discussions during the course of this work, and to Dr Mark Hallworth who provided invaluable assistance in the preparation and execution of the experiments. L. M.-E. was supported by Trinity College and financial support for O.M.P. to visit and work in Cambridge was provided by EPSRC in a grant to H.E.H. The hospitality extended by Trinity College to O.M.P. during the summer of 2001 is also gratefully acknowledged.

REFERENCES

Chan, C. L., Chen, W.-Y. & Chen, C. F. 2002 Secondary motion in convection layers generated by lateral heating of a solute gradient. *J. Fluid Mech.* **455**, 1–20.

Chen, C. F., Briggs, D. G. & Wirtz, R. A. 1971 Stability of thermal convection in a salinity gradient due to lateral heating. *Intl J. Heat Mass Transfer* **14**, 57–65.

Goldstein, S. 1938 *Modern Developments in Fluid Dynamics*. Clarendon.

Howard, L. N. & Veronis, G. 1992 Stability of salt fingers with negligible diffusivity. *J. Fluid Mech.* **239**, 511–522.

Huppert, H. E. & Turner, J. S. 1980 Ice blocks melting into a salinity gradient. *J. Fluid Mech.* **100**, 367–384.

Imberger, J., Thompson, R. & Fandry, C. 1976 Selective withdrawal from a finite rectangular tank. *J. Fluid Mech.* **78**, 489–512

Jeevaraj, C. G. & Imberger, J. 1991 Experimental study of double-diffusive instability in sidewall heating. *J. Fluid Mech.* **222**, 565–586.

Knoblock, K., Proctor, M. R. E. & Weiss, N. O. 1992 Heteroclinic bifurcations in a simple model of double-diffusive convection. *J. Fluid Mech.* **239**, 273–292.

Malki-Epshtein, L. 2005 Growth and structure of double-diffusive intrusions. PhD Thesis, Institute of Theoretical Geophysics, DAMTP, University of Cambridge.

Phillips, O. M. 1977 *The Dynamics of the Upper Ocean*. Cambridge University Press.

Ruddick, B. 1992 Intrusive mixing in a Mediterranean salt lens–intrusion slopes and dynamical mechanisms. *J. Phys. Oceanogr.* **22**, 1274–1285.

Ruddick, B. R., Phillips, O. M. & Turner, J. S. 1999 A laboratory and quantitative model of finite-amplitude thermohaline intrusions. *Dyn. Atmos. Oceans* **30**, 71–99.

Ruddick, B. R. & Turner, J. S. 1979 The vertical length scale of double-diffusive intrusions. *Deep-Sea Res.* **26A**, 903–913.

Rudnick, D. L. & Mattin, J. P. 2002 On the horizontal density ratio in the upper ocean. *Dyn. Atmos. Oceans* **36**, 3–21.

Shirtcliffe, T. G. L. & Turner, J. S. 1970 Observations of the cell structure of salt fingers. *J. Fluid Mech.* **41**, 707–719.

Thorpe, S. A., Hutt, P. K. & Soulsby, R. 1969 The effect of horizontal gradients on thermohaline convection. *J. Fluid Mech.* **38**, 375–400.